Tech Science Press

Investigation of Coronavirus Deposition in Realistic Human Nasal Cavity and Impact of Social Distancing to Contain COVID-19: A Computational Fluid Dynamic Approach

Mohammad Zuber[1], John Valerian Corda[1], Milad Ahmadi[2], B. Satish Shenoy[1], Irfan Anjum Badruddin[3,*], Ali E. Anqi[3], Kamarul Arifin Ahmad[4], S. M. Abdul Khader[5], Leslie Lewis[6], Mohammad Anas Khan[7] and Sarfaraz Kamangar[3]

[1]Department of Aeronautical & Automobile Engineering, Manipal Institute of Technology, Manipal Academy of Higher Education, Manipal, 576104, India
[2]Department of Mechanics of Solids, Surfaces and Systems, Faculty of Engineering Technology, University of Twente, Enschede, 7522, The Netherlands
[3]Mechanical Engineering Department, College of Engineering, King Khalid University, Abha, 61421, Saudi Arabia
[4]Department of Aerospace Engineering, Universiti Putra Malaysia, Serdang, 43400, Malaysia
[5]Department of Mechanical and Manufacturing Engineering, Manipal Institute of Technology, Manipal Academy of Higher Education, Manipal, 576104, India
[6]Department of Paediatrics, Kasturba Medical College & Hospital, Manipal, 576104, India
[7]Department of Mechanical Engineering, Jamia Millia Islamia, Delhi, 110025, India
*Corresponding Author: Irfan Anjum Badruddin. Email: magami.irfan@gmail.com
Received: 16 November 2020; Accepted: 27 November 2020

Abstract: The novel coronavirus responsible for COVID-19 has spread to several countries within a considerably short period. The virus gets deposited in the human nasal cavity and moves to the lungs that might be fatal. As per safety guidelines by the World Health Organization (WHO), social distancing has emerged as one of the major factors to avoid the spread of infection. However, different guidelines are being followed across the countries with regards to what should be the safe distance. Thus, the current work is an attempt to understand the virus deposition pattern in the realistic human nasal cavity and also to find the impact of distance that could be termed as a safety measure. This study is performed using Computational Fluid Dynamics as a solution tool to investigate the impact of COVID-19 deposition (i) On a realistic 3D human upper airway model and (ii) 2D social distancing protocol for a distance of 0.6, 1.2, 1.8, and 2.4 m. The results revealed that the regional deposition flux within the nasal cavity was predominantly observed in the external nasal cavity and nasopharyngeal section. Frequent flushing of these regions with saltwater substitutes can limit contamination in healthy individuals. The safe distancing limit estimated with 1 m/s airflow was about 1.8 m. The extensive deposition was observed for distances less than 1.8 m in this study, emphasizing the fact that social distancing advisories are not useful and do not take into account the external dynamics associated with airflow.

Abbreviations

CFD:	Computational Fluid Dynamics
COVID:	Coronavirus Disease
MERS:	Middle Eastern Respiratory Syndrome
SARS:	Severe Acute Respiratory Syndrome
RANS:	Reynolds Average Navier Stokes
SST:	Shear Stress Transport
CT:	Computed Tomography
LPM:	Litres Per Minute
URTI:	Upper Respiratory Tract Infections
PPE:	Personal Protective Equipment
WHO:	World Health Organization
NPI:	Non-Pharmaceutical Interventions

1 Introduction

The newly discovered variant of Coronavirus disease (COVID-19) is fast spreading. Although it was first reported in a province in China, no country is now safe from its contagious impact. Its span and reach have far exceeded the recent other pandemics such as SARS, HINI, and bird flu. Currently, no specific vaccines are available that can treat this disease. In the last two decades, SARS-CoV from 2002 to 2003, and H1N1 in 2009 have created health emergencies. The other diseases related to coronavirus, such as Middle East respiratory syndrome coronavirus (MERS-CoV) was first reported in Saudi Arabia in 2012 [1]. The novel Coronavirus disease was initially reported from Wuhan in China [2]. To date, there has not been any success with regards to vaccines or treatments for COVID-19. As on June 19, 2020, the virus has infected close to 8.32 million people leading to the death of 449,182 individuals worldwide, with the USA being the country hit hardest by this pandemic, according to a WHO report [3].

The droplets of saliva or discharge from the nose are the prime reasons for the COVID-19 virus spread. The coughs or sneezes of an infected person are responsible for most of the virus discharge, in addition to touching the surfaces on which the viruses are exhaled [4]. Studies showed that the nebulizer generated COVID-19 particulates less than 5 microns remained feasible, indicating that the virus can be transmitted partly by a small nanoparticle [5]. A study conducted using a laser light scattering approach indicates the evidence of droplets emitted during normal speaking and that these droplets remain suspended for a few minutes, which may also possibly carry virus particles in closed and confined spaces [6]. Airborne transmission is known to be the route of infection for several diseases, including tuberculosis, smallpox, and severe acute respiratory syndrome (SARS), and now this pandemic COVID-19 is also highly likely that it spreads by air [7]. In a detailed review, Li et al. [8] had observed that the ventilation and indoor air movements have a strong bearing on the transmission & spread of infection. The best way to prevent and slow down transmission is to keep a safe distance and adopt social distancing strategies. The center for disease control and prevention has suggested a safe distance of at least 6 ft. (approx. 1.8 m) from other people to avoid contamination. According to the study by Prem et al. [9], physical distancing reduces the transmissibility and incubation period of COVID-19. The study of the seasonal spread of COVID-19 cases indicates that the transmission predominantly

increases at lower relative humidity [10,11]. A study by Backer et al. [12] provides empirical evidence for the incubation period of 0 to 14 days assumed by the WHO and of 2 to 12 days assumed by the CDC.

The bio mist particles containing pathogens of various sizes are produced during the strong airflow of sneeze and cough blows [13]. Expired pathogens in the air could be inhaled into the lungs of a second individual, promoting transmission by respiration [14]. These nano-scaled airborne particulates become entrained in the airflow and get deposited deep into the respiratory system, leading to serious health problems [15]. A study by Deng et al. [16] on the deposition of coarse and fine particles showed that the coarse particles (greater than 2.5 microns) deposited tracheobronchial region whereas the finer particles (less than 2.5 microns) deposited deep in the pulmonary region. Recent studies using a realistic geometry of human oral airway have been successfully used to study the deposition patterns by Ahmadi et al. [17]. Riazuddin et al. [18], Inthavong et al. [19] and Wang et al. [20] also showed the deposition efficiency of aerosol particles in the nasal cavity for light breathing. In the study by Shi et al. [21] and Shanley et al. [22], high deposition particles were located at the anterior nasal cavity. A recent study by Ahmadi et al. [17] identified that the prominent deposition pockets are the nasal valve and vestibule regions of the nasal cavity. Thus, it is essential to understand the distribution pattern of these particulates and correctly estimate the location in the upper respiratory tract. The upper airways are the first line of defense against any respiratory infection. The anatomical structure of the nasal cavity not only serves the respiration but also has features that can filter bacteria and particulates from reaching the lungs. This is precisely the reason why the COVID deposition study is essential. Therefore, from this proposed study, it should be possible to determine the nature of COVID-19 deposition locations and intensity, which may help reduce the risk of transmission. Studies have shown that the appropriate hygienic measures, such as gargling, can prevent the spread of the virus from reaching the lungs [23]. WHO's in an article on "Cleaning and hygiene tips to help keep the COVID-19 virus out of your home" recommends the hygienic measures to be taken for personal hygiene [24]. Thus, understanding the critical deposition regions and its intensity can help reduce the contamination of a healthy human by following proper protocols.

In this study, Computational Fluid Dynamics (CFD) approach is used to visualize and compare the effects of airborne COVID-19 nano-sized particulate deposition. Two types of studies are carried out. The first study is a 3D CFD analysis of COVID-19 deposition inside a realistic human airway. A flux of 10, 100, and 1000 COVID-19 particles are injected into the human airway through the nostrils to identify the regions of deposition. The second case deals with the social distancing protocol by evaluating the various contamination distances between 2 individuals. A 2D CFD simulation is carried out for distances of 0.6, 1.2, 1.8 and 2.4 m, and the particulates were tracked to identify the amount of COVID-19 deposition that could reach the target from the source of contamination.

2 Methods

2.1 Air Flow Theory

Fundamentally CFD simulations are carried out based on a set of equations that govern the dynamics of fluids, which are essentially the mathematical forms for the conservation of laws of physics, which consists of one continuity, three momentum, and an energy equation. These collectively are called as Navier stokes equations of the airflow.

The continuity and momentum conservation equations are listed below as Eqs. (1) and (2)

$$\frac{\partial u_i}{\partial x_i} = 0 \tag{1}$$

$$u_j \frac{\partial u_i}{\partial x_j} = -\frac{1}{\rho} \frac{\partial p}{\partial x_i} + \frac{\partial}{\partial x_j} \left((v + v_t) \frac{\partial u_i}{\partial x_i} \right) \tag{2}$$

where u_i represents the air velocity in three Cartesian coordinate directions, i.e., $i = 1, 2$, and 3, ρ is the fluid density and v the kinematic viscosity, p indicates the pressure, and v_t is the kinematic turbulent (eddy) viscosity.

A turbulence model is used to compute the eddy viscosity, and the analysis assumes the airflow to be incompressible and steady. RANS model with "Turbulent Flow, SST" which is believed to provide reliable calculations involving wall-bound flows predominantly at higher separation regions, is used in this simulation. SST is a combination of the merits of both the $k - \omega$ and $k - \epsilon$ models and is widely used in the CFD community. Near wall region requires a $k - \omega$ turbulence model as it is more robust and accurate, whereas the $k - \omega$ turbulence model is accurate in the far-field where the flow involves streamlines curvatures.

2.2 Virus Particle Phase Modelling

Lagrangian particle tracking approach is employed to track individual virus particles. Force balance equations are integrated on the particles as below

$$\frac{du_p}{dt} = F_D \left(u_g - u_p \right) + \frac{g(\rho_p - \rho_g)}{\rho_p} + F_S \tag{3}$$

where

$$F_D = \frac{18u_g}{\rho_p d_p^2} \frac{C_D Re_p}{24} \tag{4}$$

$$Re_p = \frac{\rho_p d_p \left| u_p - u_g \right|}{\mu_g} \tag{5}$$

$$C_D = a_1 + \frac{a_2}{Re_p} + \frac{a_3}{Re_p{}^2} \tag{6}$$

In the above equations, a's are the empirical constants spanning over a range of Reynolds numbers for smooth spherical particles [25]. The second term of the right-hand side in Eq. (3) is the gravity term and the 3rd term F_S indicates other probable forces like basset force, virtual mass force, lift force, pressure gradient force, thermophoretic force, Brownian force which does not apply to microparticles with $\rho_p \gg \rho_g$.

The solution strategy adopted in the simulation was similar to that used by other researchers [20,26]. For the present study, the lift force, basset force, virtual mass force, pressure gradient force, thermophoretic force, is negligible and is not included in the equation. Additionally, the following assumptions have been used during computation: (a) All contaminated particles are of spherical solid shape (b) Heat and mass transfer between air and contaminated particles trajectory are neglected (c) Contaminated particles are assumed to be of uniform diameter.

(d) The virus is assumed to have identical properties of water, which is how the ejection of these particles are released via sneezing or coughing.

2.3 Modelling and Meshing

2.3.1 Nasal Cavity

The 3D model of the nasal cavity, as shown in Fig. 1, was identical to the one that was used for previous work involving the study of airflow distribution [17,27–29]. Experimental validation of this model has been carried out, and the outcomes and findings can be found in previous works by Zubair et al. [28]. The CT scanned images were segmented using MIMIC (Materialise, Ann Arbor, MI) with a requirement of adequate threshold values to differentiate the bone from the nasal wall, which varies marginally from one case to the other. Geometric enhancement of this 3D masked data was further carried out in CATIA (Dassault Systems, SÁ) and hybrid mesh consisting of unstructured tetrahedral elements at the core in addition to the prism layers at the wall was developed with y+ values less than 3. The model was solved for airflow rate of 10 LPM.
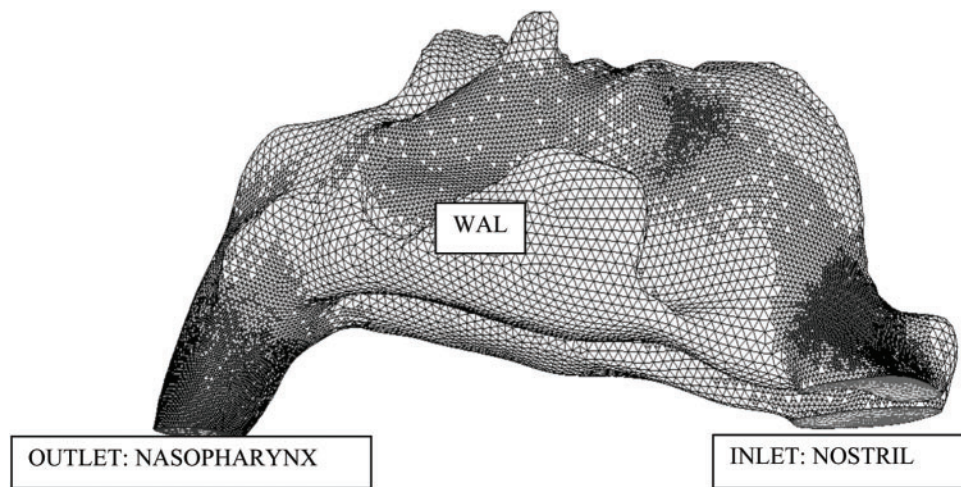
Figure 1: A 3D computational model of the human nasal cavity [27]

Commercial CFD solver COMSOL Multiphysics was used for the steady-state numerical simulation in 3D analysis for the flow inside the nasal cavity. The system capabilities were the Intel (R) Core (TM) i7-5200U CPU@2.20 GHz, 2 cores, which took approximately 2 days of runtime for the entire simulation.

The methodology employed was in accordance with previous investigations [17,18]. The SST k-ω turbulence model, which was developed by Menter [30], was employed in this simulation. This is a two-equation turbulence model, and the experimental validation by Mylavarapu et al. [31] and Ahmad et al. [32] ensures the suitability to use the SST $k - \omega$ model. The RANS turbulence model was validated by Zubair et al. [27].

The nasal wall is assumed rigid to be in addition to no-slip condition. Nostrils are given a specified mass flow rate, and nasopharynx considers no pressure outflow. Gravity is ignored, and the simulation is done with an inspiratory flow rate of 10 LPM. Results are validated with those obtained by previous researchers [33].

2.3.2 Social Distancing Protocol Study

In the wake of the COVID-19 pandemic being spread globally, the WHO recommends social distancing of at least 1 m to be adhered to. According to the Centre for Disease Control and Prevention, a distance of 6 ft (approx. 1.8 m) between people is required to avoid the possibility of picking the exhaled virus from an infected person (who may be asymptotic) in the event of uncovered coughing or sneezing. CDC defines social distancing as "To practice social or physical distancing stay at least 6 feet (about 2 arms' length) from other people" [34] On the other hand WHO mandates the distance to be maintained as "Maintain at least 1 metre (3 feet) distance between yourself and others" [35]. Onsite experimental investigation study by Niu et al. [36] showed the presence of approximately 7% of exhaust air from the lower rooms even at lower windy conditions.

A 2D steady analysis is carried out to simulate the social distancing and identify the particle tracking over a distance. Simulations are carried out for 0.6, 1.2, 1.8, and 2.4 m. These distances taken roughly come up to 2, 4, 6, and 8 ft, respectively. The numerical steady-state simulation in 2D was carried out using commercial CFD solver ANSYS Fluent 2019 R2. The schematic layout is as shown in Fig. 2, and the distance between the source and target is maintained as 2, 4, 6, and 8 ft. The source is injected with an inlet velocity of 6 m/s, indicating the contamination. Target signifies the location where the contaminations are analyzed to be deposited. The target mimics the inhalation similar to the human nasal cavity by defining a negative pressure gradient. Simulation is carried out at two different ambient velocities of 1 m/s and 0.1 m/s. The pressure outlet is maintained at 0 Pa. Wall conditions are defined for the bottom wall representing the ground, and the top section is provided with a pressure of 0 Pa. In the vicinity of the source and the target, wall conditions are maintained. Fig. 2 also shows the boundary conditions adopted for this study.
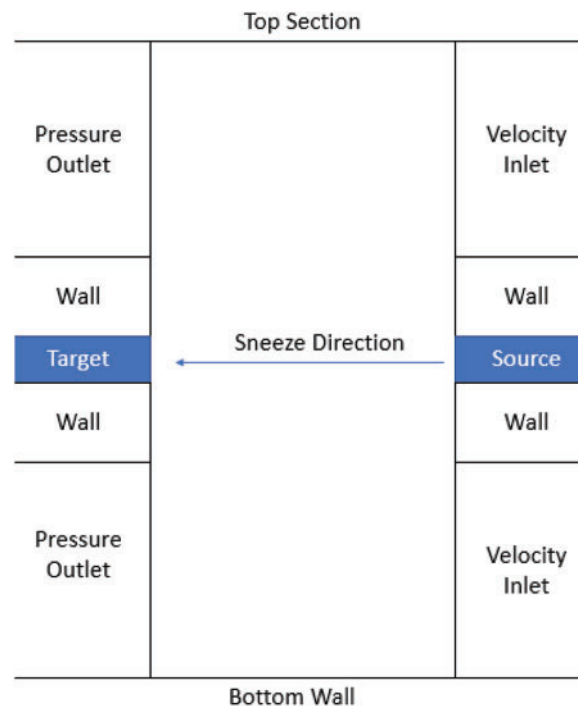
Figure 2: Schematic layout for social distancing simulation

Generation of 2D model and meshing using quadrilaterals is carried out in ANSYS Fluent 2019 R2.

3 Results and Discussion

3.1 Nasal Cavity

The accuracy of the particle tracking procedure inside the 3D nasal cavity has been established as reported by Ge et al. [33] The flow and particle transport in the entrance region of a pipe are simulated and the results obtained are compared with Ge et al. [33] The COVID-19 virus deposition efficiency in the range of 1–100 nm was simulated for a flow rate of 10 LPM. Tab. 1 illustrates the comparison of the simulated results with that of the experimental data given by Ingham et al. [37], and the numerical investigation by Ge et al. [33]. Although the Eulerian species simulation is valid for small nanoparticles, Xi et al. [38] have shown that with increased flow rate and particle size, the particle inertia becomes essential. According to Ge et al. [33], the trend of deposition efficiency for 1 LPM and that of 10 LPM flow rate are similar.

Table 1: The deposition efficiency for 100 nm particles in a straight pipe (1 LPM; Re = 322)

Particles size	1 nm	10 nm	100 nm
Ingham et al. [37]	0.79	0.55	NA
Ge et al. [32]	0.83	0.57	0.3
Present study	0.81	0.53	0.29

The 3D nasal model used in this study was the same that was used in earlier studies by Zubair et al. [28]. The model has been experimentally validated and is reproduced from our previous study. The compilation of velocity contours at various locations inside the nasal cavity, as shown in Fig. 3, provides a distinct explanation for airflow distribution. It indicates the regions of high-velocity regions represented by color legend with 1.6 m/s to 2 m/s representing a higher velocity region, which is the nasal valve region. The nasal valve is the narrowest part of the airways and connects the external noise with the internal nasal cavity consisting of turbinate. Also, the flow is seen to be developing as it approaches the nasopharyngeal section.

The primary objective of this present study was to mimic the COVID-19 deposition inside the upper airways. The previously developed 3D patient-specific nasal cavity was utilized to model the deposition patterns of the COVID-19 virus. Previous studies have estimated the size of the COVID-19 to be approximately 100 nm [39]. A stream of these virus particles was injected into the nasal cavity through the nostrils and its deposition regions obtained. The particles were assumed to be spherical, and the virus was considered to be inert having identical properties as that of the sneeze water droplets. Tab. 2 shows the deposition efficiency of the COVID-19 at 10 LPM and compared with that with identical particulate sized deposition efficiency available in the literature. The deposition efficiency for 100 nm COVID-19 particles is of the same order as that reported by Ge et al. [33] and Cheng et al. [26].

Fig. 4 presents the location of COVID-19 deposition regions. It also indicates the salient regions of COVID-19 deposits inside the upper airways. The vestibule and the nasopharyngeal section of the nose are the most important locations for deposition. This has been established by earlier researchers who have also shown the vestibule and external region of the upper airways to have higher depositions. In the present study, the influence of nasal hair and mucous has

been neglected. It is expected to have higher deposits due to porosity induced by nasal cilia and mucous, which has the ability to retain more particulates.
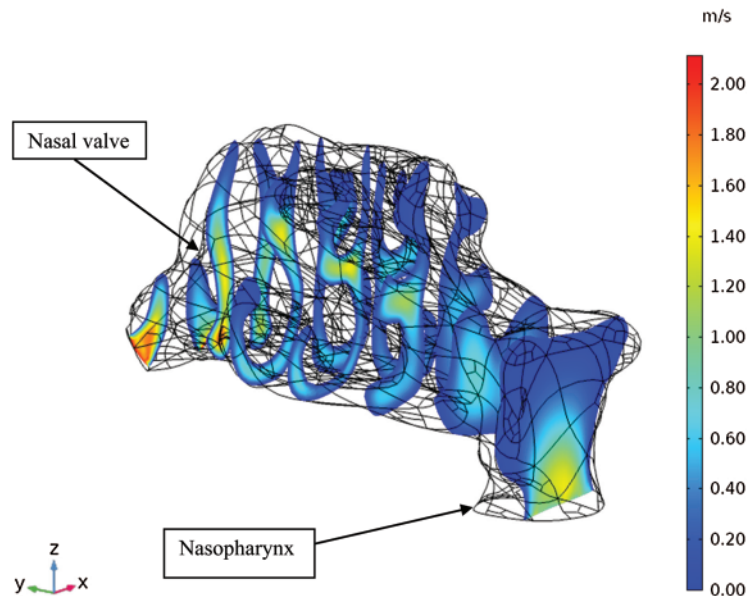
Figure 3: Velocity contour at various sections inside the nasal cavity

Table 2: Comparison of deposition efficiency of COVID-19 at 10 LPM

Description	Deposition efficiency (%)
Wang et al. [20]	11.765
Zamankhan et al. [40]	13.472
Cheng et al. [26]	3.415
Ge et al. [33]	4.75
Present study	6.23

Fig. 5 provides a comparison of the percentage of COVID-19 particulates deposited at various locations inside the nasal cavity. The locations presented account for more than 75% of the deposition areas within the nose. It can also be noted that the external nose alone can trap about 45% of the virus particles effectively. The external nose and the nasopharyngeal sections together account for almost 60% of the total deposits. The COVID-19 samples in nasal and throat swabs obtained from the 17 symptomatic patients in Zhuhai, Guangdong, China showed higher viral loads detected in the nose than in the throat [41]. This corroborates the findings from the current study, which shows that the external nose accounts for higher virus loads. It can be inferred from these findings that, if these 2 locations are periodically cleaned, the ability of the virus to reach the lower airways can be drastically reduced. It can be advised to clean the nose with saline water, and gargling should suffice to clear the throat of these impurities. This should help mitigate the effect of COVID-19 to a considerable extent. A randomized control trial consisting of 387 samples showed that simple water gargling was effective in preventing upper respiratory

tract infections (URTI) among healthy people [23]. Gargling may be more effective for pathogens, which predominantly colonize the oropharynx. To be effective, it must be frequently carried out. Non-pharmaceutical interventions (NPIs) such as hand hygiene are beneficial when vaccination is insufficient or not available [42]. A review by King et al. [43] reported that saline nasal irrigation might have some benefit in patients with acute upper respiratory tract infections. The use of Normal saline water and salt water drops (thrice/day) helped reduce the severity of symptoms of upper respiratory tract infections in young children. In a pilot study by Ramalingam et al. [44], hypertonic saline nasal irrigation and gargling significantly reduced the duration of URTI. This virtually cost-free modality can help healthy individuals from contaminating the COVID-19 virus to a large extent.
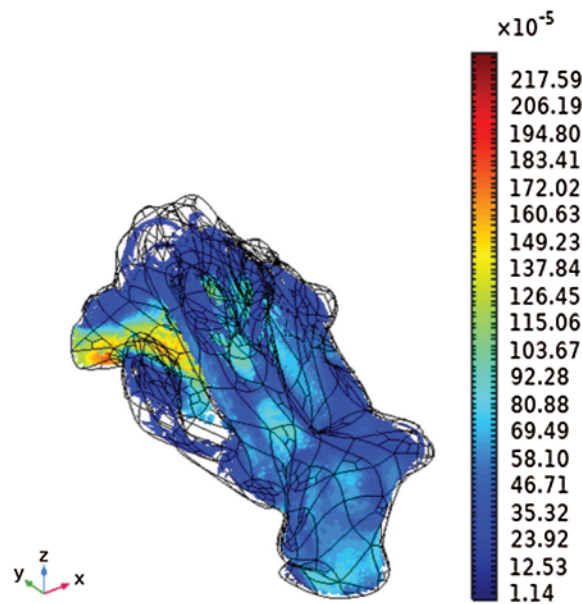
Figure 4: Upper airway deposition regions for COVID-19
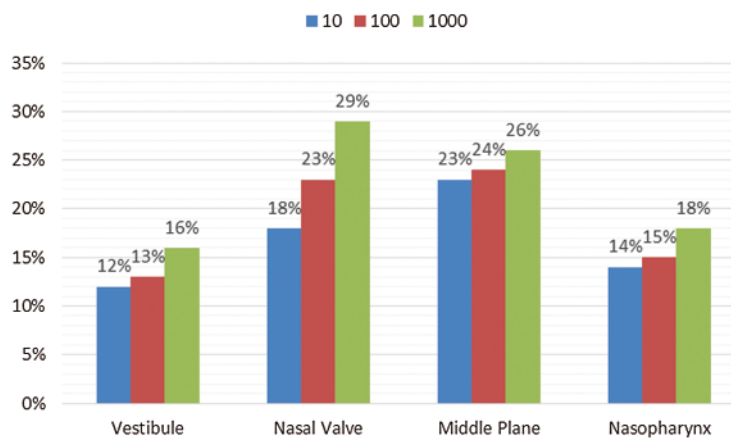
Figure 5: Percentage deposition of COVID-19 particles in different regions of the nasal cavity

Fig. 5 also indicates the flux of 10, 100 and 1000 particles injected into the nasal cavity and their deposition locations. It is observed that the highest deposition is at the nasal valve region, which is a constricted region in the nasal cavity. This is followed by the middle plane region, which accounts for a quarter of total depositions.

The nasal valve which is the most constricted part of the nasal cavity plays an important role in trapping a part of the contaminants. Below Tab. 3 shows the different regions in the nasal cavity and the particle deposition percentages. This indicates the critical region in the nasal cavity that is the nasal valve which traps about a third of the virus and requires special attention and frequent cleaning using saline water to flush out the virus deposited.

Table 3: Percentage deposition in different zones in the nasal cavity

Region	Percentage deposition (%)
Vestibule	16
Nasal valve	29
Mid plane	26
Nasopharynx	18

3.2 Social Distancing Protocol

Onsite investigation after the SARS outbreak revealed the influence of the exhaust air on pathogen transport [36]. These pathogens can, in turn, contaminate the people and lead to a cascade of cases associated with work or hospital setup. While sneezing, about 40,000 droplets are generated of 0.5–12 μm in diameter [45]. On the other hand, a person coughing can produce around 3000 droplets [46]. During normal breathing, sneezing can project droplets to several meters [45].

The recent outbreak of coronavirus (COVID-19) has forced us to re-visit our social distancing protocols. According to the study by Prem et al. [9], physical distancing reduces the transmissibility and incubation period of COVID-19 [36] In this study, a 2D analysis of the spread of the virus from cough/sneeze has been simulated to identify the safer distance between the source of COVID-19 and healthy individuals. In this study, the virus load for 0.6, 1.2, 1.8, and 2.4 m are investigated.

Fig. 6 quantifies COVID-19 particles that can be inhaled by the healthy individual for various distances from the source of contaminant. In this case study, a near-silent wind velocity of 0.1 m/s was adopted to mimic the best-case scenario avoiding external flow dynamics. In a comprehensive survey by Baldwin et al. [47], it was shown that the mean value of airflow speeds in indoor workplaces was 0.3 m/s. It was observed that, under these idealistic conditions, the depositions were observed only for a distance of 0.6 m (approximately 2 ft). There was no deposition for distances beyond 0.6 m.

On the other hand, when the indoor conditions are influenced by higher airflow rates (1 m/s), the social distancing protocol suggested by WHO fails to contain the spread of the virus. It is clearly observed in Fig. 7 that, even with a distance of 1.2 m, a large swath of virus deposition is obtained. However, beyond 1.8 m, there was no deposit, which concurs with the suggestion of the Centre for Disease Control and Prevention for a safe distancing of at least 6 ft.
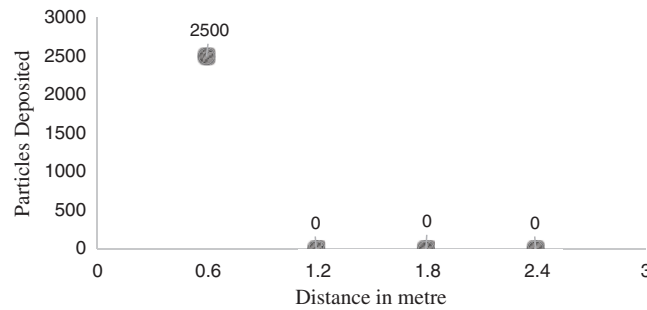
Figure 6: Nasal deposition *vs.* distance for wind velocity $= 0.1$ m/s
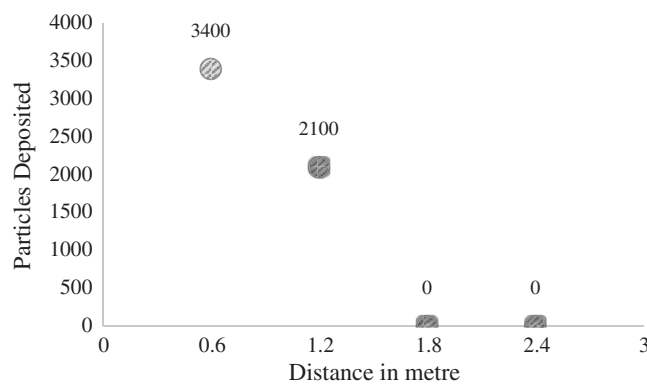
Figure 7: Nasal deposition *vs.* distance for wind velocity $= 1$ m/s

Some of the external conditions, such as temperature, moisture content, and particle inhalability, have been ignored in the present study. However, expectedly for such conditions, the deposition amount would be higher than that as predicted in this work. A series of experimental studies conducted by Bjørn et al. [46] using manikins and combining standing and sitting positions indicated that the exhalation jet penetrated the breathing zone of a nearby person with high magnitude of concentrations making social distancing necessary. Although Qian et al. [48], has experimentally established that the aerosols from the patient have the ability to spread long distances under the displacement type ventilation system. Similarly, Kao et al. [49] used computational fluid dynamical method and demonstrated that airflow patterns and air exchange rates have a significant effect on control of airborne virus diffusion. A CFD simulation to identify the spreading mechanisms of exhaled pollutants like the SARS virus indicate a possibility of cross infections due to long distances of sneezing [50]. Thus, social distancing advisory cannot be the only metric to avoid contamination. As the present study demonstrates, the change in external dynamics can lead to contamination despite social distancing. Thus, the relaxation towards the human movement for restarting economic activities should be reconsidered carefully. Though social distancing is a significant consideration in order to avoid the spread of COVID-19, other factors like the use of PPE, frequently washing hands, avoiding contacts of contaminated hands to eyes, nose, and mouth could prevent the virus from entering the human system.

The present study deals with the nasal depositions in the absence of PPE, like the face mask and face shield. Further studies can be carried out by considering the effectiveness of PPEs in containing the virus from entering the nasal cavity. Additionally, the distribution of the

contaminations (virus) in a closed room, laboratory, schools, or college setup can be studied, and means for reduction of the same by proper ventilation of the rooms can be proposed.

4 Conclusion

The impact of social distancing on COVID-19 deposition in the nasal cavity has been investigated in the present study. Numerical simulation has been carried on a realistic 3D nasal cavity to understand the COVID-19 deposition distribution. Deposition patterns indicate a significant percentage of COVID-19 particles getting accumulated at the nasal vestibule and the nasal valve region of the nasal cavity. Besides, the influence of social distancing on COVID-19 has been simulated at a different distance of 0.6, 1.2, 1.8, and 2.4 m. At low ambient velocity, the COVID-19 depositions were observed only for a distance of 0.6 m, and there was no deposition for distances beyond 0.6 m, which agrees with some of the experimental observations. On the contrary, at higher ambient velocity, the social distancing protocol failed to contain the spread of the virus, and a large swath of virus deposition is obtained even with a distance of 1.2 m. However, beyond 1.8 m, there were no deposits, which agrees well with Centre for Disease Control and Prevention protocol of maintaining a social distance of 2 m as safe distancing. Thus, the social distancing advisory cannot be the only metric to avoid contamination of COVID-19.

Conflict of Interest: The authors declare that they have no conflicts of interest to report regarding the present study.

References

1. Cascella, M., Rajnik, M., Cuomo, A., Dulebohn, S. C., Napoli., R. D. (2020). *Features, evaluation and treatment coronavirus (COVID-19)*. Treasure Island (FL): StatPearls Publishing.
2. Xu, Z., Shi, L., Wang, Y., Zhang, J., Huang, L. et al. (2020). Pathological findings of COVID-19 associated with acute respiratory distress syndrome. *Lancet Respiratory Medicine, 8(4),* 420–422. DOI 10.1016/S2213-2600(20)30076-X.
3. WHO Coronavirus Disease (COVID-19) Dashboard (2020). https://covid19.who.int/table.
4. Morawska, L. (2006). Droplet fate in indoor environments, or can we prevent the spread of infection? *Indoor Air, 16(5),* 335–347. DOI 10.1111/j.1600-0668.2006.00432.x.
5. van Doremalen, N., Bushmaker, T., Morris, D. H., Holbrook, M. G., Gamble, A. et al. (2020). Aerosol and surface stability of SARS-CoV-2 as compared with SARS-CoV-1. *New England Journal of Medicine, 382(16),* 1564–1567. DOI 10.1056/NEJMc2004973.
6. Stadnytskyi, V., Bax, C. E., Bax, A., Anfinrud, P. (2020). The airborne lifetime of small speech droplets and their potential importance in SARS-CoV-2 transmission. *Proceedings of the National Academy of Sciences, 117(22),* 11875–11877. DOI 10.1073/pnas.2006874117.
7. Droegemeier, K. (2020). *Rapid Expert Consultation on the Possibility of Bioaerosol Spread of SARS-CoV-2 for the COVID-19 Pandemic*. National Academies of Sciences, National Academies Press (US), https://www.ncbi.nlm.nih.gov/books/NBK556967/.
8. Li, Y., Leung, G. M., Tang, J. W., Yang, X. Chao, C. Y. H. et al. (2007). Role of ventilation in airborne transmission of infectious agents in the built environment: A multidisciplinary systematic review. *Indoor Air, 17(1),* 2–18. DOI 10.1111/j.1600-0668.2006.00445.x.
9. Prem, K., Liu, Y., Russell, T. W., Kucharski, A. J., Eggo, R. M. et al. (2020). The effect of control strategies to reduce social mixing on outcomes of the COVID-19 epidemic in Wuhan, China: A modelling study. *Lancet Public Health, 2667(20),* 1–10. DOI 10.1016/S2468-2667(20)30073-6.

10. Ward, M. P., Xiao, S., Zhang, Z. (2020). The role of climate during the COVID-19 epidemic in New South Wales, Australia. *Transboundary and Emerging Diseases, 26(6),* 0–2. DOI 10.1111/tbed.13631.

11. Luo, W., Majumder, M. S., Liu, D., Poirier, C., Mandl, K. D. et al. (2020). The role of absolute humidity on transmission rates of the COVID-19 outbreak. *MedRxiv,* 2020.02.12.20022467. DOI 10.1101/2020.02.12.20022467.

12. Backer, J. A., Klinkenberg, D., Wallinga, J. (2020). Incubation period of 2019 novel coronavirus (2019-nCoV) infections among travellers from Wuhan, China, 20–28 January 2020. *Eurosurveillance, 25(5),* 1–6. DOI 10.2807/1560-7917.ES.2020.25.5.2000062.

13. Nishimura, H., Sakata, S., Kaga, A. (2013). A new methodology for studying dynamics of aerosol particles in sneeze and cough using a digital high-vision, high-speed video system and vector analyses. *PLoS One, 8(11),* e80244. DOI 10.1371/journal.pone.0080244.

14. Fiegel, J., Clarke, R., Edwards, D. A. (2006). Airborne infectious disease and the suppression of pulmonary bioaerosols. *Drug Discovery Today, 11(1–2),* 51–57. DOI 10.1016/S1359-6446(05)03687-1.

15. King Se, C. M., Inthavong, K., Tu, J. (2010). Inhalability of micron particles through the nose and mouth. *Inhalation Toxicology, 22(4),* 287–300. DOI 10.3109/08958370903295204.

16. Deng, Q., Deng, L., Miao, Y., Guo, X., Li, Y. (2019). Particle deposition in the human lung: Health implications of particulate matter from different sources. *Environmental Research, 169,* 237–245. DOI 10.1016/j.envres.2018.11.014.

17. Ahmadi, M., Kojourimanesh, M., Zuber, M., Riazuddin, V. N., Khader, S. M. A. (2019). CFD analysis of mucous effect in the nasal cavity. *Journal of Computational Methods in Sciences and Engineering, 19(2),* 491–498. DOI 10.3233/JCM-181006.

18. Riazuddin, V. N., Zubair, M., Ahmadi, M., Tamagawa, M., Rashid, N. H. A. et al. (2016). Computational fluid dynamics study of airflow and microparticle deposition in a constricted pharyngeal section representing obstructive sleep apnea disease. *Journal of Medical Imaging and Health Informatics, 6(6),* 1507–1512. DOI 10.1166/jmihi.2016.1839.

19. Inthavong, K., Tu, J., Ahmadi, G. (2009). Computational modelling of gas-particle flows with different particle morphology in the human nasal cavity. *Journal of Computational Multiphase Flows, 1(1),* 57–82. DOI 10.1260/175748209787387061.

20. Wang, S. M., Inthavong, K., Wen, J., Tu, J. Y., Xue, C. L. (2009). Comparison of micron- and nanoparticle deposition patterns in a realistic human nasal cavity. *Respiratory Physiology and Neurobiology, 166(3),* 142–151. DOI 10.1016/j.resp.2009.02.014.

21. Shi, H., Kleinstreuer, C., Zhang, Z. (2007). Modeling of inertial particle transport and deposition in human nasal cavities with wall roughness. *Journal of Aerosol Science, 38(4),* 398–419. DOI 10.1016/j.jaerosci.2007.02.002.

22. Shanley, K. T., Zamankhan, P., Ahmadi, G., Hopke, P. K., Cheng, Y. S. (2008). Numerical simulations investigating the regional and overall deposition efficiency of the human nasal cavity. *Inhalation Toxicology, 20(12),* 1093–1100. DOI 10.1080/08958370802130379.

23. Satomura, K., Kitamura, T., Kawamura, T., Shimbo, T., Watanabe, M. et al. (2005). Prevention of upper respiratory tract infections by gargling: A randomized trial. *American Journal of Preventive Medicine, 29(4),* 302–307. DOI 10.1016/j.amepre.2005.06.013.

24. UNICEF (2020). *Cleaning tips to help keep COVID-19 out of your home.* https://www.unicef.org/coronavirus/cleaning-and-hygiene-tips-help-keep-coronavirus-COVID-19-out-your-home.

25. Morsi, S. A., Alexander, A. J. (1972). An investigation of particle trajectories in two-phase flow systems. *Journal of Fluid Mechanics, 55(2),* 193–208. DOI 10.1017/S0022112072001806.

26. Cheng, Y. S., Yeh, H. C., Guilmette, R. A., Simpson, S. Q., Cheng, K. H. et al. (1996). Nasal deposition of ultrafine particles in human volunteers and its relationship to airway geometry. *Aerosol Science and Technology, 25(3),* 274–291. DOI 10.1080/02786829608965396.

27. Zubair, M., Riazuddin, V. N., Abdullah, M. Z., Rushdan, I., Shuaib, I. L. et al. (2013). Computational fluid dynamics study of pull and plug flow boundary condition on nasal airflow. *Biomedical Engineering—Applications, Basis and Communications, 25(4),* 1–8. DOI 10.4015/S1016237213500440.

28. Zubair, M., Arifin, K., Mohd, A., Abdullah, Z. (2015). Characteristic airflow patterns during inspiration and expiration: Experimental and numerical investigation. *Journal of Medical and Biological Engineering, 35(3),* 387–394. DOI 10.1007/s40846-015-0037-4.

29. Riazuddin, V. N., Zubair, M., Abdullah, M. Z., Ismail, R., Shuaib, I. L. et al. (2011). Numerical study of inspiratory and expiratory flow in a human nasal cavity. *Journal of Medical and Biological Engineering, 31(3),* 201–206. DOI 10.5405/jmbe.781.

30. Menter, F. R. (1994). Two-equation eddy-viscosity turbulence models for engineering applications. *AIAA Journal, 32(8),* 1598–1605. DOI 10.2514/3.12149.

31. Mylavarapu, G., Murugappan, S., Mihaescu, M., Kalra, M., Khosla, S. et al. (2009). Validation of computational fluid dynamics methodology used for human upper airway flow simulations. *Journal of Biomechanics, 42(10),* 1553–1559. DOI 10.1016/j.jbiomech.2009.03.035.

32. Ahmad, K. A., Abdullah, M. Z., Watterson, J. K. (2010). Numerical modelling of a pitching airfoil. *Jurnal Mekanikal, 30,* 37–47.

33. Ge, Q. J., Inthavong, K., Tu, J. Y. (2012). Local deposition fractions of ultrafine particles in a human nasal-sinus cavity CFD model. *Inhalation Toxicology, 24(8),* 492–505. DOI 10.3109/08958378.2012.694494.

34. CDC (2020). Coronavirus Disease 2019 (COVID-19). *Centers for disease control and prevention*, https://www.cdc.gov/coronavirus/2019-ncov/prevent-getting-sick/social-distancing.html.

35. WHO Web Page (2020), https://www.who.int/emergencies/diseases/novel-coronavirus-2019/advice-for-public.

36. Niu, J., Tung, T. C. W. (2008). On-site quantification of re-entry ratio of ventilation exhausts in multi-family residential buildings and implications. *Indoor Air, 18(1),* 12–26. DOI 10.1111/j.1600-0668.2007.00500.x.

37. Ingham, D. B. (1975). Diffusion of aerosols from a stream flowing through a short cylindrical pipe. *Journal of Aerosol Science, 6(2),* 125–132. DOI 10.1016/0021-8502(75)90005-1.

38. Xi, J., Longest, P. W. (2008). Numerical predictions of submicrometer aerosol deposition in the nasal cavity using a novel drift flux approach. *International Journal of Heat and Mass Transfer, 51(23–24),* 5562–5577. DOI 10.1016/j.ijheatmasstransfer.2008.04.037.

39. Kim, J., Chung, Y., Jun, H., Lee, N., Seon, M. et al. (2020). Identification of Coronavirus Isolated from a Patient in Korea with COVID-19. *Osong Public Health and Research Perspectives, 11(1),* 3–7. DOI 10.24171/j.phrp.2020.11.1.02.

40. Zamankhan, P., Ahmadi, G., Wang, Z., Hopke, P. K., Cheng, Y. S. et al. (2006). Airflow and deposition of nano-particles in a human nasal cavity. *Aerosol Science and Technology, 40(6),* 463–476. DOI 10.1080/02786820600660903.

41. Zou, L., Ruan, F., Huang, M., Liang, L. Huang, H. et al. (2020). SARS-CoV-2 viral load in upper respiratory specimens of infected patients. *New England Journal of Medicine, 382(12),* 1–3. DOI 10.1056/NEJMc2001737.

42. Aiello, A. E., Murray, G. F., Perez, V., Coulborn, R. M., Davis, B. M. et al. (2010). Mask use, hand hygiene, and seasonal influenza-like illness among young adults: A randomized intervention trial. *Journal of Infectious Diseases, 201(4),* 491–498. DOI 10.1086/650396.

43. King, D., Mitchell, B., Williams, C. P., Spurling, G. K. P. (2015). Saline nasal irrigation for acute upper respiratory tract infections. *Cochrane, Database of Systematic Reviews, 4,* DOI 10.1002/14651858.CD006821. pub3.

44. Ramalingam, S., Graham, C., Dove, J., Morrice, L., Sheikh, A. (2019). A pilot, open labelled, randomised controlled trial of hypertonic saline nasal irrigation and gargling for the common cold. *Scientific Reports, 9(1),* 1–11. DOI 10.1038/s41598-018-37703-3.

45. Cole, E. C., Cook, C. E. (1998). Characterization of infectious aerosols in health care facilities: An aid to effective engineering controls and preventive strategies. *American Journal of Infection Control, 26(4),* 453–464. DOI 10.1016/S0196-6553(98)70046-X.

46. Bjørn, E., Nielsen, P. V. (2002). Dispersal of exhaled air and personal exposure in displacement ventilated rooms. *Indoor Air, 12(3),* 147–164. DOI 10.1034/j.1600-0668.2002.08126.x.

47. Baldwin, P. E. J., Maynard, A. D. (1998). A survey of wind speeds. *Indoor Workplaces, 42(5),* 303–313.

48. Qian, H., Li, Y., Nielsen, P. V., Hyldgaard, C. E., Wong, T. W. et al. (2006). Dispersion of exhaled droplet nuclei in a two-bed hospital ward with three different ventilation systems. *Indoor Air, 16(2),* 111–128. DOI 10.1111/j.1600-0668.2005.00407.x.

49. Kao, P. H., Yang, R. J. (2006). Virus diffusion in isolation rooms. *Journal of Hospital Infection, 62(3),* 338–345. DOI 10.1016/j.jhin.2005.07.019.

50. Gao, N., Niu, J. (2006). Transient CFD simulation of the respiration process and inter-person exposure assessment. *Building and Environment, 41(9),* 1214–1222. DOI 10.1016/j.buildenv.2005.05.014.